

Edge-Driven Phase Transitions in 2D Ice

Suchit Negi, Alexandra Carvalho,* Maxim Trushin, and A. H. Castro Neto



Cite This: *J. Phys. Chem. C* 2022, 126, 16006–16015



Read Online

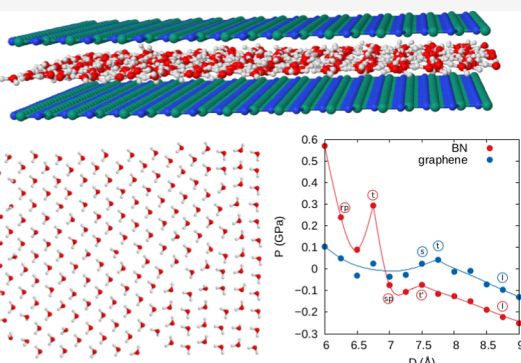
ACCESS |

Metrics & More

Article Recommendations

Supporting Information

ABSTRACT: Two-dimensional (2D) water, confined by atomically flat layered materials, may transit into various crystalline phases even at room temperature. However, to gain full control over the crystalline state, we should not only confine water in the out-of-plane direction but also restrict its in-plane motion, forming 2D water clusters or ribbons. One way to do this is by using an electric field, in particular the intrinsic electric field of an adjacent polar material. We have found that the crystalline phases of 2D water clusters placed between two hexagonal boron nitride (h-BN) nanoribbons are crucially determined by the nanoribbons' edges, the resulting polarity of the nanoribbons, and their interlayer distance. We make use of the density functional theory with further assistance of molecular dynamics simulations to establish the comprehensive phase diagrams, demonstrating transitions between liquid and solid phases and between the states of different crystalline orders. We also show that the crystalline orders are maintained when water flows between h-BN channels under external pressure. Our results open a promising pathway toward the control of the water structure and its flow by the use of the microscopic electric field of polar materials.



1. INTRODUCTION

Water has always been a subject of interest in account of its unusual properties and its universal importance across the fields of science and engineering. Its phase diagram contains at least 18 ice phases in addition to the most known I_h ice,¹ with some of them still being the object of research. Besides, water can be supercooled and undergo glass transitions to “glassy” amorphous water states.² Moderately confined water, similar to supercooled water, is prevented from crystallizing at low temperatures,^{3,4} and has long been the object of research due to its importance for biological,⁵ pharmaceutical, and food industry applications. Most recently, however, water confined at the nanometer scale has been shown instead to display the long-range order characteristic of an “ice” even at room temperature.^{6–12}

Nanoconfined water is usually studied either in carbon nanotubes^{13,14} realizing one-dimensional (1D) confinement or in graphene slits squeezing water down to a two-dimensional (2D) monolayer.^{6–8,15–17} The flat geometry of the latter makes it possible to impose an additional in-plane confinement and study transition between not only bulk and 2D states but also 2D and 1D limits by having a finite channel. The edge effects are then of ultimate importance.

As the majority of critical processes in molecular biology occur in confined water, they must essentially depend on the water structure at the molecular scale.¹⁸ The role of water structure is perhaps most apparent in the folding of protein chains, binding of some proteins to substrates, and aggregation of proteins into functional units.^{19,20} When proteins do all that,

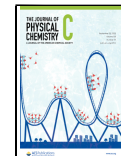
the intervening water molecules must shift out of the way, breaking the water structure. The result is therefore determined by the forces maintaining the water structure. Thus, the ability to control the water structure at the molecular level is fundamental for the development of biochemistry and biotechnology processes.

When a polar crystal such as h-BN is finite, it can have a permanent dipole moment depending on its geometry. Previous theoretical studies have considered the effect of the B–N bond polarity on the water confined by nanotubes,^{21,22} on surfaces,^{23,24} or in wide channels.²⁵ However, the structure and phase diagram of monolayer water confined by BN sheets has not been considered before. As we will describe in the present article, monolayer 2D water can exhibit different crystalline phases if it is confined by finite boron nitride ribbons. Most of the 2D ice forms predicted so far have no macroscopic electric dipole,^{7,8,16,17} similar to 3D ices, which are typically anti-ferroelectric, with the exception of the polar phases XI and XIX.¹ In this article, we show that 2D water confined by finite, polar h-BN nanoribbons has at least two polar ice phases that are stable at room temperature.

Received: June 29, 2022

Revised: August 29, 2022

Published: September 13, 2022



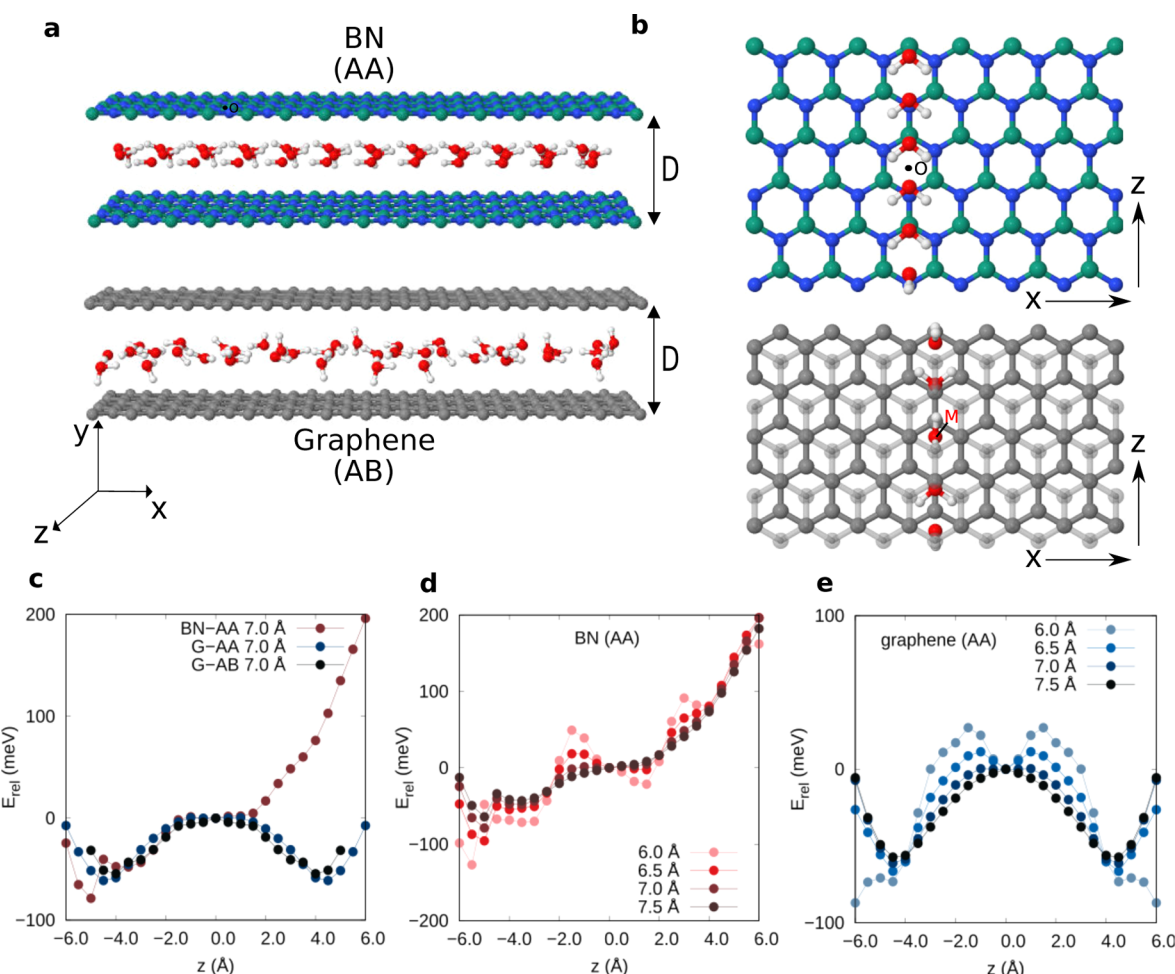


Figure 1. Edge effects on the orientation and energy of a single water molecule placed in between h-BN or graphene nanoribbons: (a) schematic illustration of the semi-infinite channel made of graphene or boron nitride layers, periodic along the x direction, and with length L measured along the z direction. The monolayer of water appears to be more structured in the case of a boron nitride confinement. (b) Lowest energy configurations of a water molecule at different z for $D = 7 \text{ \AA}$ (diagrammatic montage); only the bottom h-BN layer is shown for clarity. Nitrogen, boron, carbon, oxygen, and hydrogen atoms are represented by blue, green, gray, red, and white spheres, respectively. (c) Relative energy of a water molecule confined by h-BN or graphene in either AA or AB stacking for an inter-layer spacing of 7 \AA ; z is measured from point "O"/"M". (d) Relative energy of a water molecule for different inter-layer distances for AA-stacked h-BN; (e) relative energy of a water molecule for different inter-layer distances for AA-stacked graphene.

We start by examining the energetics of water confined between finite layers using density functional theory (DFT) calculations. We then use equilibrium molecular dynamics (MD) simulations to describe the structure of 2D water between finite or infinite h-BN or graphene sheets in a wider range of conditions, and offer a qualitative explanation of the edge effect along with an effective electrostatic model. Finally, we examine the structure of water in stationary flow.

2. METHODS

2.1. DFT Calculations. First-principles DFT calculations were carried out using the Quantum ESPRESSO package.²⁶ The VDW-DF1 exchange and correlation energy functional was used.²⁷ This exchange functional has been previously tested for hydrogen-bonded systems with accurate results.²⁸ Ultrasoft pseudo-potentials were used to account for the core electrons.²⁹ We employed a plane wave basis set with kinetic energy cutoffs of 35 Ry to describe the electronic wave functions. The Brillouin zone was sampled using a Γ -centered $4 \times 4 \times 1$ Monkhorst-Pack (MP) grid³⁰ for all calculations.

2.2. Classical MD. The classical MD simulations were performed using the LAMMPS code.³¹

Many classical potentials for water have been proposed in the literature. We have employed the reparameterized simple point charge model (SPCE) model,³² for which water–BN interactions have been determined by Wagemann et al. (SPCE/WWDM).²³ Alternatives are TIP4P and TIP3P, for which water–BN interactions have been determined by Wu et al. (WWA)³³ and Hilder et al. (HYGGBRC),³⁴ respectively. We could not test TIPSP because we did not find BN interaction parameters for this potential in the literature. The water–carbon interaction was modeled by a Lennard-Jones potential between oxygen and carbon atoms.

We employed the SPCE water model, which is known to give very good structural parameters and self-diffusion constant for 3D water.³⁵ The SPCE water model has also previously been used to study the phase diagram of 2D water using the method that we adopted in the present paper, with results consistent with experiment.⁸ We found this model to be in reasonable agreement with DFT for strictly planar 2D water (Supporting Information, Section S2.2). All the three

potentials considered favor SQ with respect to RP for strictly 2D water, however, by a small energy margin ([Supporting Information, S2](#)). Thus, the disappearance of the non-polar SQ phase from the phase diagram of water confined by BN nanoribbons cannot be attributed to limitations of the classical potential. A comparison of the main results of this paper for different classical potentials can be found in [Supporting Information, S3](#).

The water–BN interaction parameter of Wageman et al.²³ employed here consists of a Lennard-Jones potential between oxygen and boron or nitrogen. These result in a contact angle of 73°. The results for different water–BN interacting potentials were found to be consistent (see [Supporting Information, S3](#)), except when using the potential of Hilder et al.,³⁴ due to the large N and B charges in the latter (± 0.98), which are larger than previous estimates (<0.3) for similar structures.³⁶

Long-range Coulomb forces were computed using the particle–particle particle-mesh method. Water molecules were kept at a constant temperature of 300 K using a Nosé–Hoover thermostat with a damping constant of 10 fs (100 timesteps). The graphene or boron nitride atoms were not coupled to the thermostat. A timestep of 0.1 fs was used.

3. RESULTS AND DISCUSSION

3.1. Energetics of Water Confined in 1D \leftrightarrow 2D

Channels. Previous studies of 2D water have usually assumed a structure that is periodic along both in-plane directions. However, in reality, both the confining layers and the water in between are finite and have edges. We can use this effect to our advantage as a mean to further control the structure of the water.

We will consider a water channel formed by two semi-infinite graphene or boron nitride layers, as shown in [Figure 1a](#). The channel's in-plane width (W), along the x direction is assumed to be infinite (periodic), and the channel's height (the interlayer distance D), along the y direction, is a few Å. If the distance between edges (i.e., the channel's length L , along the z direction) was comparable to the size of the water molecules, the system would become 1D. In contrast, if L was infinite, the system would become 2D. We study systems with $10 < L < 400$ Å, which are at the 1D \rightarrow 2D transition.

For the purpose of illustrating the effect of the h-BN polarization on the water, we will use stoichiometric, semi-infinite nanoribbons with asymmetric zigzag edges, that is, one edge is N-terminated, whereas the opposite one is B-terminated, such as the one represented in [Figure 1b](#). The top and down h-BN flakes are stacked in AA configuration. We choose this configuration because it allows us to maximize the polarization of the channel with the edges aligned at $z = 0$ and $z = L$. This will be further supported by the electrostatic model in [Section 3.6](#). In reality, the channels can be mechanically stacked in many other configurations, but as long as the finite layers are asymmetric with respect to inversion, there will be a finite polarization. We start by investigating the potential energy landscape for water molecules confined in such channels. For comparison, we carried out similar calculations for graphene, stacked in either AB or AA configurations, both of which have no net polarization.

The nanoribbons used were semi-infinite and, unless otherwise specified, consisted of a total of 168 atoms with a width of 11.3–11.5 Å for the AA-stacked structures, and 140 atoms with a width of 10.0 Å for AB-stacked structures. The

supercell size used was $17.5 \times 35.0 \times 30.0$ Å³. The relative energies were found to change less than 1 meV when the vacuum spacing was increased by 5 Å along y or z . Spin polarization of the edges was taken into account (for more details, please see the [Methods](#) section).

3.2. Edge Effects on a Single Water Molecule. A single water molecule confined between h-BN nanoribbons spontaneously reorients itself so that its dipole is anti-parallel to the polarization of the ribbons. The difference in energy between the parallel and anti-parallel dipoles, for a water molecule placed at equal distance from the two borders (site “O” in [Figure 1b](#)) is 0.13 and 0.11 eV for inter-layer distances of 6 and 7 Å, respectively. In contrast, in graphene the two orientations are symmetrically equivalent.

However, close to the border of the h-BN confining layers, the orientation of the water molecule is no longer dictated by the polarization but rather by the local atomic environment. The energy and orientation of the water molecule at different distances from the border, obtained by fixing the oxygen position to different coordinates along the z axis, are shown in [Figure 1b](#). There are three effects to have into consideration: (i) the position of the atoms of the water molecule with respect to the atoms of the lattice of the 2D materials on both sides, (ii) the position of the water molecule with respect to the border, and (iii) the orientation of the water dipole with respect to the polarization of the nanoribbon.

A comparison between different stackings and between polar/non-polar NRs shows that the polarization (iii) is the most important factor shaping the potential energy landscape ([Figure 1](#)). We define the relative energy of the water molecule, referenced to its energy at $z = 0$, as $E_{\text{rel}}(z) = E_{\text{tot}}(z) - E_{\text{tot}}(0)$, where E_{tot} is the total energy calculated using DFT. The respective energy profile is nearly identical for the water molecules confined between AA- or AB-stacked graphene sheets ([Figure 1c](#)).

The lowest energy position for adsorption of a water molecule on a single graphene sheet³⁷ or in between AA-stacked sheets is at the hexagonal site (“O”). The difference in energy between the hexagonal sites at the center and at the border is about 70 meV (independently of the inter-layer spacing).

In the case of AA-stacked h-BN, the lowest energy position for the oxygen is also close to the center of the hexagonal ring. For $z < 0$, the energy profile resembles that of the water molecule between graphene sheets. However, there is now a strong asymmetry in z due to the polar nature of the h-BN nanoribbons. The variations of the potential energy of the molecule across the surface are more pronounced for the smaller inter-layer distances ([Figure 1d,e](#)).

The water molecule prefers different orientations with respect to the confining layers depending on the distance to the border and to the confining layer atoms. In the case of confinement by h-BN, the water molecule always prefers to be parallel to the confining layers, except when it is close to a border nitrogen atom, in which case it can orient itself perpendicularly to the layers in order to form hydrogen bonds with the nitrogen atoms. In the case of graphene, however, the water molecule adopts different orientations depending on the closest graphene lattice sites. This difference, as we will see, contributes to the increased order in water phases formed at the 1D \leftrightarrow 2D transition in h-BN channels.

3.3. Confined Water Clusters. We now use tetra-water clusters to investigate the relative strength of the water–water

interactions. These small water clusters share the same square or rhombic local motifs as the most relevant 2D water phases, a consequence of the maximization of the number of hydrogen bonds between water molecules. However, different from an infinite 2D water layer, water molecules are not all fully bonded, with four hydrogen bonds per molecule.

Tetra-water clusters are confined by semi-infinite nanoribbons with zigzag edges similar to those described in the previous section. The most relevant configurations are shown in Figure 2. The clusters SQ1 and SQ2 are nearly planar. In

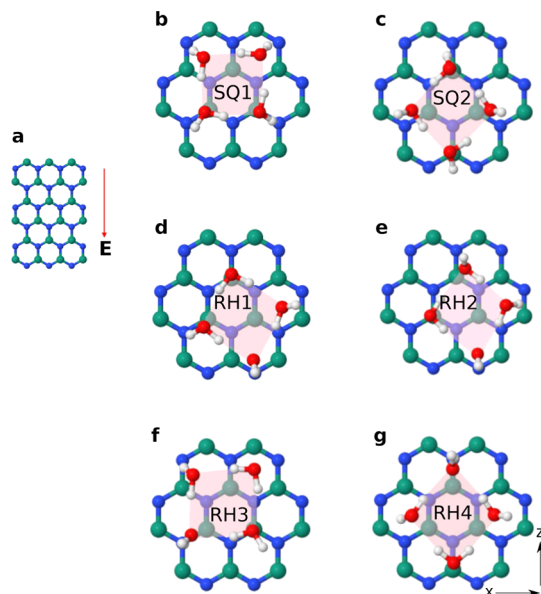


Figure 2. Water clusters confined by finite-size h-BN nanoribbons. (a) Orientation of the h-BN nanoribbon. The nanoribbons are infinite along the horizontal direction. E indicates the direction of the intrinsic electric field. (b–g) Tetra-water clusters in different configurations, see Table 1 for the relative energies. The top h-BN layer is hidden, for clarity.

contrast, in the RH1–RH4 clusters, one of the molecules is oriented vertically, forming hydrogen bonds with N because it is unable to form hydrogen bonds with the other water molecules. Note that this is not common in infinite water layers, as the hydrogen bonding with O is preferred to hydrogen bonding with N, which is less electronegative. All the configurations shown have four hydrogen bonds between water molecules, but SQ1 and SQ2, where each water molecule has one and only one H atom involved in a hydrogen bond (Table 1).

We estimate the average hydrogen bond energy as $E_H = [E_{4H_2O} - 4E_{1H_2O}]/4$, where E_{4H_2O} is the energy of the tetra-water cluster, at fixed atomic positions, without the presence of BN, and E_{1H_2O} is the energy of a single water molecule. E_H is larger for SQ1 and SQ2, indicating that the larger the number of hydrogen bonds established by a water molecule, the weaker they become.

Comparing our estimates of the energy scales of the interactions involved in the water layer formation, we find that hydrogen bonds are the strongest, with energies in the range 50–250 meV, followed by the dipole reorientation energy (<110 meV) and border proximity effects (100 meV). Comparatively, the local changes of potential energy due to proximity to the $B,N/C$ atoms far from the border are small

Table 1. Relative Energies of Tetra-water Xlusters (E_{rel}) Confined by h-BN or Graphene Layers, along with the Average Hydrogen Bond Energy (E_H), for an Inter-Layer Distance of 7 Å^a

structure	h-BN (AA)		graphene (AB)	
	E_{rel}	E_H	E_{rel}	E_H
SQ1	0	245	1	249
SQ2	5	253	0	256
RH1	8	149	94	147
RH2	relaxes to RH1	149	242	154
RH3	115	151	244	154
RH4	334	150	94	145

^aAll energies are given in meV.

(<50 meV), especially for inter-layer distances of 7.0–7.5 Å. Taking this into account, it is not surprising that 2D water forms water phases that maximize the formation of hydrogen bonds. At room temperature, it favors square and rhombic phases instead of forming phases commensurate with the confining lattice. In the following sections, we will study such 2D water phases and how they change at the 2D \leftrightarrow 1D transition.

3.4. Phases of Confined 2D Water. We used classical MD simulations to explore the phase diagram of 2D water at 300 K. AA-stacked h-BN layers and AB-stacked graphene layers were chosen as model systems. The phase diagrams are calculated at room temperature for different distances between plates (D) and lateral pressures. The MD simulations are performed at constant number of particles (N), with water covering given area A , determined by the size of the h-BN supercell. For a given N , we calculate the pressure on the (virtual) supercell walls perpendicular to the walls separation, $P(D)$. Phase transitions between the different phases accessible to the system can be identified by a non-monotonic change of $P(D)$ with D at constant N .⁸ The procedure is similar to what has been used in ref 8 and our outcomes are consistent with previous results for water confined by graphene layers (see Supporting Information, S1). We focus mostly on the regions of stability of monolayer water, in either the solid or liquid state, and under compression. Further details about the MD simulations can be found in the Methods section.

A comparison between the classical potentials and DFT for the system studied in the previous section can be found in Supporting Information, S2. While the classical potentials perform poorly when comparing the energies of water clusters with one or two hydrogen water molecules, they perform better for fully bonded water phases. We have chosen the classical potential SPC/E.³² This model gives the best structural parameters and self-diffusion constant among the most commonly used nonpolarized classical water models.³³ The impact of the classical water model chosen will be discussed in more detail in the next sections.

Infinite boron-nitride sheets, modeled using periodic boundary conditions along both in-plane directions, have no net intrinsic electric field, and the phases of water confined by such sheets are identical to those found when water is confined by graphene (Figure 3a). The main crystalline phase encountered is the square phase (S), as shown in Figure 3b, which has been observed in previous experiments⁶ and predicted theoretically.^{7–12} However, the situation is different when water is confined by polar BN nanoribbons.

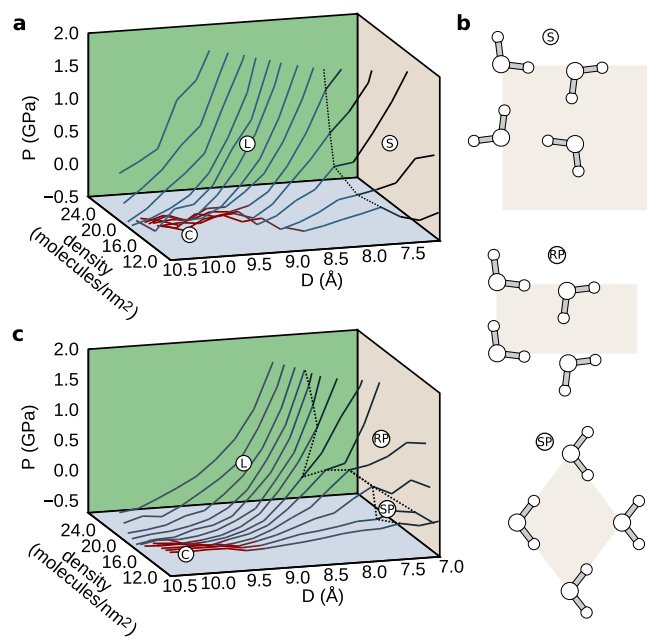


Figure 3. Phase diagrams for water confined by either (a) infinite h-BN sheets or (c) finite h-BN nanoribbons. The liquid, non-polar square, rhombic polar, and square polar phases are designated by “L”, “S”, “RP”, and “SP”, respectively. “C” indicates cavitation. (b) Schematic illustration of the crystalline water phases (not to scale).

3.5. Between 2D and 1D: Confinement by h-BN Nanoribbons. We now consider 2D water nanoribbons, which can be viewed as a quasi-1D system, obtained by confining the 2D water in between h-BN nanoribbons. These

ribbons, in the xOz plane, are finite along z and infinite along x . The channel’s length (L) is approximately 42 Å. The supercell is 65.1 and 63.9 Å wide (the channel’s width W) along the x direction for h-BN and graphene, respectively. The water is kept in the confined region by perfectly reflective wall boundaries placed parallel to the nanoribbon edges.

2D water confined between h-BN nanoribbons shows two distinct solid phases. These are a rhombic polar (RP) phase and a square polar (SP) phase. For a density of about 12 molecules/ nm^2 (the density of the 2D square ice observed experimentally⁶), the transition between the two solid phases occurs at $D = 6.75 \text{ \AA}$. Below $D = 6.50 \text{ \AA}$, there is a rhombic phase where the oxygen atom arrangement shows rhombus motifs (Figure 4a). This is the same as the rhombic structure proposed in ref 17, except that we did not observe the duplication of the unit cell at room temperature. The electrical dipoles of the O–H bonds are approximately parallel to the z direction pointing to the N-terminated edge, such that the net polarization of the water layer is opposed to that of the h-BN nanoribbon. At $D = 6.75 \text{ \AA}$, there is a phase transition, with domains of the two phases coexisting (Figure 4b). Above this transition point, the square polar phase, where the electric dipole of each water molecule is aligned with the $-z$ direction, becomes the most stable (Figure 4c,d). This phase is the same as the “PR” (puckered rhombic) phase proposed in.³⁸ Besides, in all regions of the phase space, there are structural changes near the N-terminated zigzag edge.

Water confined by the graphene nanoribbon, in contrast, only shows a solid–liquid transition at $D = 7.75 \text{ \AA}$ (Figure 4e). This is similar to what has been previously found for 2D water

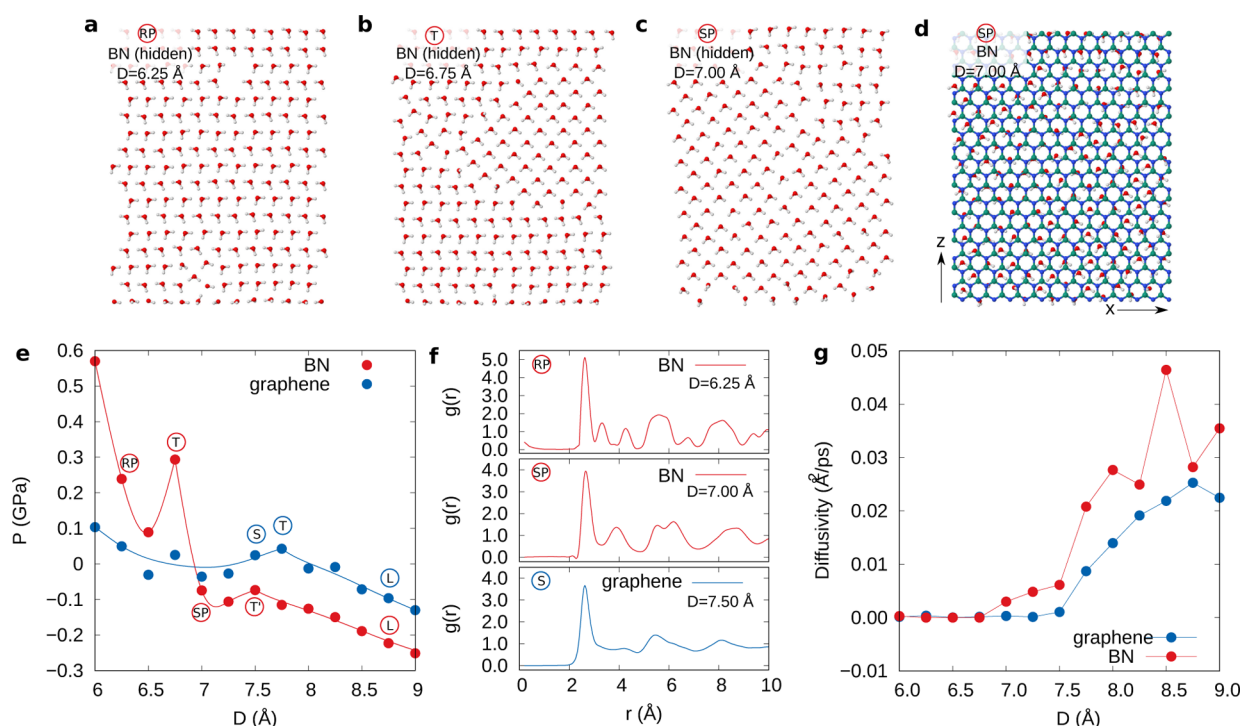


Figure 4. Phases of 2D water confined by semi-infinite monolayer h-BN or graphene nanoribbons. Structures for h-BN confinement for (a) rhombic polar phase, (b) rhombic polar and square polar phases coexisting at transition point, (c) square polar phase, and (d) square polar phase, showing the orientation of the ribbon. The respective interlayer distances D are shown in the insets; (e) phase diagram; (f) 2D RDFs [$g(r)$]; and (g) 2D diffusivity obtained from the mean square displacements. The density is 12.4 molecules/ nm^2 for graphene and 12.2 molecules/ nm^2 for h-BN.

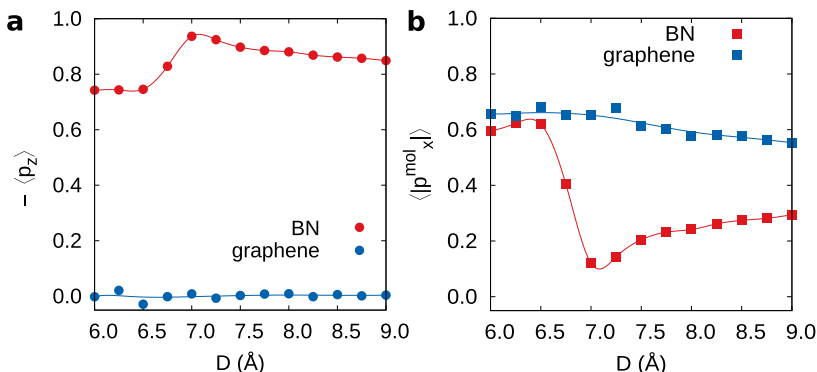


Figure 5. Averaged dipole moment per water molecule, in units of the water dipole (2.35 D for SPCE), for 2D water confined by h-BN and graphene nanoribbons: (a) average polarization of the z-component and (b) average of the absolute value of the x-component of the molecular polarizations.

confined by infinite graphene planes⁸ (see Supporting Information, S1).

The phase transitions give rise to anomalies in the $P(D)$ plots (Figure 4e). Additionally, different phases have distinct radial distribution functions (RDFs) (Figure 4f). In the rhombic polar structure, each oxygen atom has four nearest neighbors at 2.6–2.8 Å and two second nearest neighbors at 3.2–3.4 Å. In contrast, in the square polar structure, each oxygen atom also has four nearest neighbors at 2.6–2.8 Å, but there is a second distinct peak due to the four second nearest neighbors at 3.8–3.9 Å. In both the rhombic and square polar phases of water confined by the h-BN ribbons, the peaks of the RDF are sharper than those of the RDF for water confined by graphene. A phase diagram for varying molecular density and confining inter-layer distance is shown in Figure 3b.

The diffusivity is also different for the rhombic and square polar phases, being higher for the latter, and it dramatically increases in the liquid state (Figure 4g). Thus, despite some degree of disorder, especially in the H sublattice, it is clear that all the three phases observed (square, rhombic polar, and square polar) are solid at room temperature.

In order to quantify the presence of the polar phases for the 2D water, we have calculated the average electric dipole per water molecule, $\langle p \rangle$ (Figure 5). This is zero for the square water phase, but non-zero for the rhombic polar and square polar phases.

For the water confined by the h-BN nanoribbons, there is a noticeable increase of the value of $\langle p_z \rangle$ toward its maximum value at the phase transition from the rhombic polar phase to the square polar phase (Figure 5a). Even the liquid phase is highly polarized. In contrast, $\langle p_z \rangle$ is zero for the water confined by the graphene nanoribbon.

Furthermore, to help differentiating between the rhombic polar and the square polar phases, we calculated $\langle |p_x^{\text{mol}}| \rangle$, the ensemble average of the absolute values of the molecular polarization component along x . This is zero for the perfect square polar structure because all the molecules have a mirror symmetry plane parallel to xOy , but it is non-zero for the rhombic polar structure. Thus, an abrupt decrease of $\langle |p_x^{\text{mol}}| \rangle$ is observed at the phase transition from the rhombic polar phase to the square polar phase (Figure 5b). In contrast, the value of $\langle |p_x^{\text{mol}}| \rangle$ remains constant for graphene.

We note that the stabilization of polar 2D water phases in the case of h-BN confinement is not an artifact of the choice of

classical potential because, according to our tests for strictly planar 2D water phases, in Supporting Information S2.2, this model slightly penalizes the polar water phases, compared to DFT. In Supporting Information, S3.1, we show that the presence of polar solid phases and the solid to liquid transition near $D \sim 7$ Å are independent of the choice of classical potentials.

3.6. Electric Field Variation within the h-BN Nanoribbon Width. We have shown that water confined by finite h-BN nanoribbons acquires new phase states which are not present in water confined by infinite h-BN layers. We have attributed this difference to the macroscopic polarization of the nanoribbon system associated with an intrinsic electric field. The energy of a water molecule in the resulting electric field, E_{dip} , is given by $E_{\text{dip}} = -\mathbf{p} \cdot \mathbf{E} = -pE_z \cos \theta$, where \mathbf{p} is the electric dipole of the water molecule, \mathbf{E} is the electric field, which is assumed to be along the z direction, $\mathbf{E} = E_z \mathbf{e}_z$, and θ is the angle between \mathbf{p} and \mathbf{E} . We now analyze quantitatively the electric field produced by the nanoribbon and how it varies in-plane and within the nanoribbon width.

It is possible to quantify the electric field in h-BN channels by means of an equivalent electrostatic model, Figure 6a, representing the boron and nitrogen edges as linear charge distributions, with linear charge density λ of the order of 0.1 e/Å. The electric field of a single line placed at $z = z_0$, $y = \pm D/2$ reads

$$\mathbf{E} = \frac{\lambda}{2\pi\epsilon} \frac{(z - z_0)\mathbf{e}_z + (y \mp D/2)\mathbf{e}_y}{(z - z_0)^2 + (y \mp D/2)^2} \quad (1)$$

where $\mathbf{e}_{y,z}$ are the unit vectors and ϵ is the dielectric permittivity. Because the water flow is restricted to the plane, the water molecules are most sensitive to the in-plane electric field (along \mathbf{e}_z) in the middle of the interlayer gap ($y = 0$). The total in-plane electric field at mid-gap in the case of AA stacking can be written as

$$E_z^{\text{tot}} = \frac{\lambda}{\pi\epsilon} \sum_{n=0}^{N-1} \left[\frac{z - nl}{(z - nl)^2 + (D/2)^2} - \frac{z - nl - z_0}{(z - nl - z_0)^2 + (D/2)^2} \right] \quad (2)$$

where $l = 3a/2$, $z_0 = a/2$ with a bond length of $a = 1.44$ Å³⁹, and N is the number of h-BN unit cells along the channel. The $n = 0$ term corresponds to the field produced by two boron

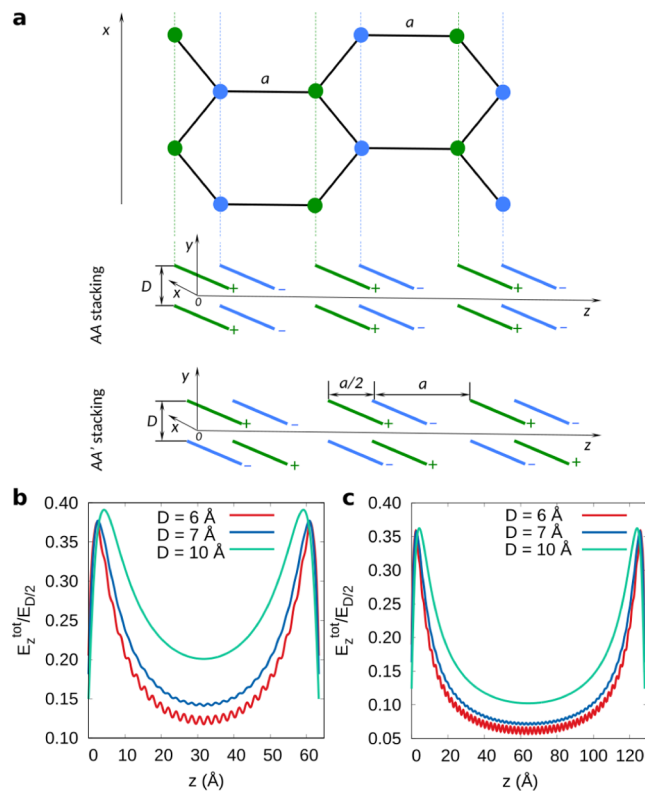


Figure 6. Effective electrostatic model for the in-plane mid-gap electric field produced by the polar h-BN nanoribbons. (a) Difference between AA and AA' stacking assemblies. The boron and nitrogen linear charge distributions are shown in green and blue, respectively. (b,c) In-plane mid-gap electric field given by eq 2 in units of $E_{D/2} = \lambda / (\pi \epsilon D)$ for AA stacking with (b) $L \sim 65 \text{ \AA}$ (30 unit cells) and (c) $L \sim 130 \text{ \AA}$ (60 unit cells). The in-plane field at the middle of the gap vanishes in the case of AA' stacking.

edges with $+\lambda$ placed at $z = 0, y = \pm D/2$ and two nitrogen nearest-neighbor lines with $-\lambda$ placed at $z = z_0, y = \pm D/2$. The $n = N - 1$ term corresponds to the field produced by two nitrogen edges placed at $z = 3aN/2 - a, y = \pm D/2$, and two boron nearest-neighbor lines placed at $z = 3a(N - 1)/2, y = \pm D/2$. Both the upper and lower h-BN layers are thus boron-terminated at $z = 0$ and nitrogen-terminated at $z = 3aN/2 - a$. The system as a whole is electrically neutral. The field contributions produced by the upper and lower h-BN layers are equivalent in the middle of the interlayer gap and sum-up to a finite value.

The total in-plane mid-gap electric field is maximal near the edges and decreases in the middle of the channel (Figure 6b,c). However, it remains comparable with the edge field if the ribbon width is of the order of 10 Å. The absolute value of the field at the channel edges is about $\lambda / (\pi \epsilon D) \sim 10^9 \text{ V/m}$. It is strong enough to fully polarize water molecules.⁴⁰ The field oscillates as a function of the z coordinate, with amplitude depending on the ratio between a and D . If $a/D \ll 1$, then oscillations are negligible.

In an MD simulation for water confined by h-BN nanoribbons of a longer length ($L = 368 \text{ \AA}$), we are able to see the ordered, polar phase within 100 Å of the edges, while at the center of the water layer the electric field vanishes, and the water layer becomes disordered (Figure 7). Near the center of the water layer, the 2D water is still polarized, although less than near the edges (see Supporting Information, S4).

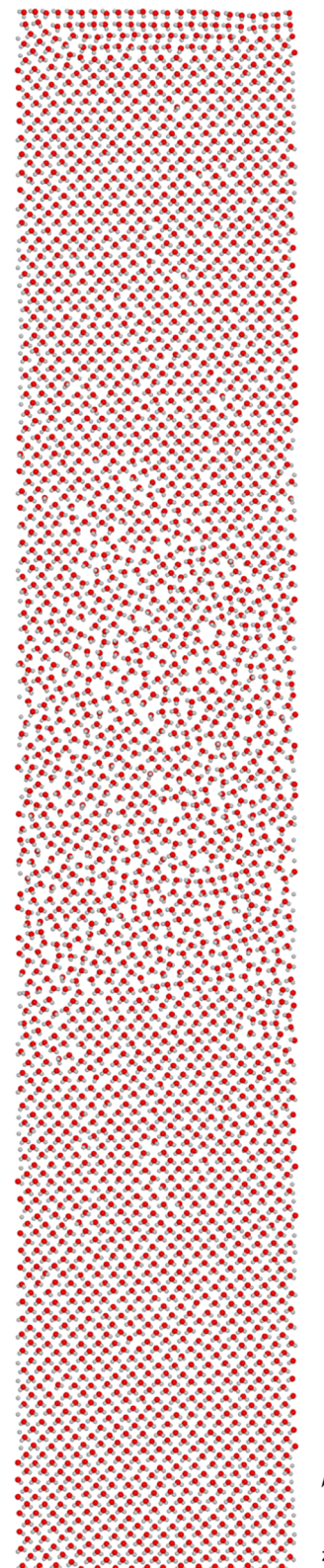


Figure 7. Snapshot of the water monolayer in a h-BN channel with width $L = 368 \text{ \AA}$ along the z direction, and $D = 7 \text{ \AA}$, along the direction perpendicular to the plane. The channel is infinite along the horizontal direction. The water density is 12.4 molecules/ nm^2 . Transition between ordered and disordered states occurs at the distance of about 100 Å from the nearest edge due to the vanishing in-plane mid-gap electric field far away from the nanoribbon's edges, see Figure 6.

In the case of AA' stacking (with top and bottom edges aligned), the situation is completely different because each term originating from a line at $y = +D/2$ is explicitly compensated by the term with $y = -D/2$ as having an opposite sign. Hence, the total in-plane mid-gap electric field vanishes in the case of AA' stacking.

From this model, we can also see that if $L \rightarrow \infty$, then the average electric field tends to zero, in agreement with the MD results shown earlier for the infinite h-BN sheet. This is therefore a nanoscale effect.

3.7. Dynamics of Confined Water Flow in Polar BN Channels. Finally, we have considered the phases of water during stationary flow in the presence of a pressure gradient. The model system is represented in Figure 8a. It consists of

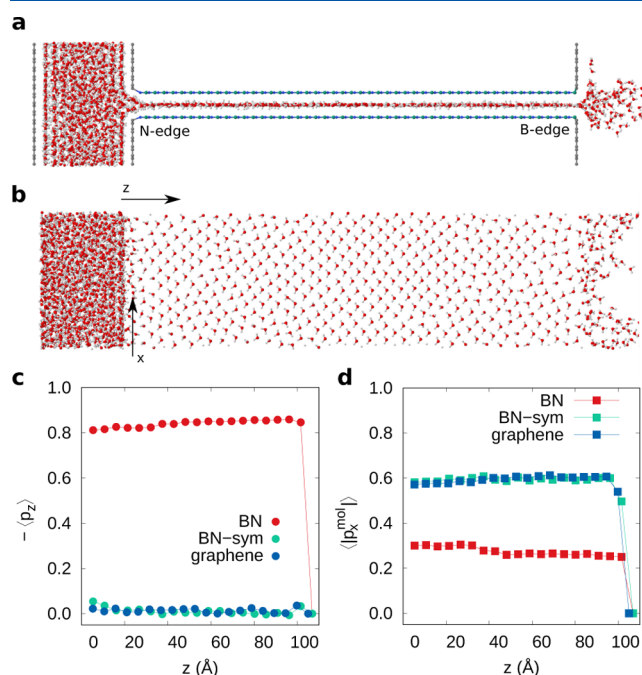


Figure 8. Structure of confined water flowing between two reservoirs with a pressure difference of $\Delta P = 10$ atm: (a) system diagram, (b) snapshot of the water structure, (c) average of the z-component of dipole moment per water molecule, in units of the water dipole (2.35 D for SPCE), and (d) average of the absolute value of the x-component of the molecular polarizations for graphene, h-BN (AA), and a centrosymmetric channel with AA' stacking (BN-sym). The channel inter-layer distance is 6 Å.

two reservoirs separated by a 2D channel with length $L = 105$ Å for graphene and $L = 108$ Å for h-BN, corresponding to the same number of repeating units. The reservoir on the left has a moving graphene piston with a total applied force $f = PA$, where A is its area. The channel consisted of either (i) two graphene sheets or (ii) two h-BN sheets with AA stacking and N-terminated edge on the $+z$ side, B-terminated edge on the $-z$ side. The inter-layer distances were 6 and 7 Å.

We considered pressure differences between the two reservoirs from 5 to 208 atm. In all cases, the water layer was in the solid state with a structured oxygen sublattice, but the O–H bonds were polarized for the water flow through the h-BN channel. This is illustrated in Figure 8c,d for a channel interlayer distance of 6 Å and a pressure difference of 10.4 atm. The density was in the range 10.8–14.9 molecules/nm² for graphene and 11.7–12.4 molecules/nm² for h-BN. The value

of $\langle p_z \rangle$ is close to the maximum polarization for h-BN, but nearly zero for graphene. There is a mixture of rhombic polarized and square polarized phases (the latter featured in Figure 8a). This is confirmed by the $\langle |p_x^{\text{mol}}| \rangle$ value, which lies between the values characteristic of these two phases. This is in contrast with the graphene confinement, for which there is no net water polarization.

4. CONCLUSIONS

DFT calculations, together with MD simulations, indicate that 2D water confined by finite h-BN nanoribbons is more ordered than when confined by identical graphene nanoribbons. The difference is mainly due to the presence of an intrinsic electric field in finite, asymmetric h-BN layers, and is not observed for water confined by infinite h-BN layers which have no net electric field. The reorientation energy of the molecules is higher close to the edges than at the center of the nanoribbon, and its average value over the whole surface vanishes as the nanoribbon width tends to infinity.

At room temperature, water confined by AA-stacked, polar h-BN layers less than 7.5 Å apart is crystalline and can assume one of two polar phases, RP and SP. The regions of confining distance where RP or SP dominate depend on the classical potential employed. When flowing due to a pressure gradient, a strong polarization of the water molecules is maintained during flow.

The qualitative results obtained here can be generalized for nanoribbons of different nanoscale widths, as long as the polarity of the top and bottom layers is the same. If they have inversion symmetry, however, no difference is expected as in the case of graphene.

The edges of the nanoribbons give us the ability to control the crystalline states of water confined in between. This approach can be further explored considering different polar materials. Even though an external electric field can change the water structure and dynamics in nanotubes^{41–44} and inorganic systems,⁴⁵ the method could be hazardous in practice. In contrast, making use of the intrinsic electric field in h-BN, which is already a typical material used in prototypes of nanodevices and nanocapillaries, opens the way to safe electrical manipulation of the water structure. The main difficulty at present is the production of BN with clean zigzag edges. Such edges have been sparsely reported even for graphene.⁴⁶ The process of edge creation would have to be compatible with the methods currently used for the creation of nanochannels by assembly of laminar 2D sheets. Nevertheless, the polar 2D water phases described here can potentially be found in regions of water intentionally or unintentionally intercalated between BN sheets during the assembly of heterostructures.

ASSOCIATED CONTENT

Supporting Information

The Supporting Information is available free of charge at <https://pubs.acs.org/doi/10.1021/acs.jpcc.2c04492>.

MD simulation of 2D water confined by infinite boron nitride sheets, comparison of DFT and classical potentials: water clusters, comparison between classical potentials: phase diagram for water confined by BN NRs, structure of 2D water confined by graphene NRs, and wide BN nanoribbon simulation (PDF)

AUTHOR INFORMATION

Corresponding Author

Alexandra Carvalho — Centre for Advanced 2D Materials, National University of Singapore, Singapore 117546, Singapore; Institute for Functional Intelligent Materials, National University of Singapore, Singapore 117544, Singapore; Email: carvalho@nus.edu.sg

Authors

Suchit Negi — Centre for Advanced 2D Materials, National University of Singapore, Singapore 117546, Singapore; Institute for Functional Intelligent Materials, National University of Singapore, Singapore 117544, Singapore; orcid.org/0000-0002-9174-8529

Maxim Trushin — Centre for Advanced 2D Materials, National University of Singapore, Singapore 117546, Singapore; Institute for Functional Intelligent Materials, National University of Singapore, Singapore 117544, Singapore; Department of Materials Science Engineering, National University of Singapore, Singapore 117575, Singapore; orcid.org/0000-0002-1407-7194

A. H. Castro Neto — Centre for Advanced 2D Materials, National University of Singapore, Singapore 117546, Singapore; Institute for Functional Intelligent Materials, National University of Singapore, Singapore 117544, Singapore; Department of Materials Science Engineering, National University of Singapore, Singapore 117575, Singapore

Complete contact information is available at:
<https://pubs.acs.org/10.1021/acs.jpcc.2c04492>

Notes

The authors declare no competing financial interest.

ACKNOWLEDGMENTS

This research/project was supported by the Ministry of Education, Singapore, under its Research Centre of Excellence award to the Institute for Functional Intelligent Materials, National University of Singapore (I-FIM, project no. EDUNC-33-18-279-V12). The computational work was supported by the Centre of Advanced 2D Materials (CA2DM), funded by the National Research Foundation, Prime Ministers Office, Singapore, under its Medium-Sized Centre Programme. M.T. thanks the Director's Senior Research Fellowship from CA2DM [R-723-000-001-281] for support.

REFERENCES

- (1) Salzmann, C. G.; Loveday, J. S.; Rosu-Finsen, A.; Bull, C. L. Structure and Nature of Ice XIX. *Nat. Commun.* **2021**, *12*, 3162.
- (2) Mishima, O.; Stanley, H. E. The Relationship between Liquid, Supercooled and Glassy Water. *Nature* **1998**, *396*, 329–335.
- (3) Ricci, M. A.; Bruni, F.; Giuliani, A. "Similarities" between confined and supercooled water. *Faraday Discuss.* **2009**, *141*, 347–358.
- (4) Cerveny, S.; Mallamace, F.; Swenson, J.; Vogel, M.; Xu, L. Confined Water As Model of Supercooled Water. *Chem. Rev.* **2016**, *116*, 7608–7625.
- (5) Acosta-Gutierrez, S.; Scorcipino, M. A.; Bodrenko, I.; Ceccarelli, M. Filtering with Electric Field: The Case of *E. coli* Porins. *J. Phys. Chem. Lett.* **2015**, *6*, 1807–1812.
- (6) Algarra-Siller, G.; Lehtinen, O.; Wang, F.; Nair, R. R.; Kaiser, U.; Wu, H.; Geim, A. K.; Grigorieva, I. V. Square Ice in Graphene Nanocapillaries. *Nature* **2015**, *519*, 443–445.
- (7) Zangi, R.; Mark, A. E. Monolayer Ice. *Phys. Rev. Lett.* **2003**, *91*, 025502.
- (8) Gao, Z.; Giovambattista, N.; Sahin, O. Phase Diagram of Water Confined by Graphene. *Sci. Rep.* **2018**, *8*, 6228.
- (9) Zhu, Y.; Wang, F.; Bai, J.; Zeng, X. C.; Wu, H. Compression Limit of Two-Dimensional Water Constrained in Graphene Nanocapillaries. *ACS Nano* **2015**, *9*, 12197–12204.
- (10) Jiang, J.; Gao, Y.; Zhu, W.; Liu, Y.; Zhu, C.; Francisco, J. S.; Zeng, X. C. First-Principles Molecular Dynamics Simulations of the Spontaneous Freezing Transition of 2D Water in a Nanoslit. *J. Am. Chem. Soc.* **2021**, *143*, 8177–8183.
- (11) Neek-Amal, M.; Peeters, F. M.; Grigorieva, I. V.; Geim, A. K. Commensurability Effects in Viscosity of Nanoconfined Water. *ACS Nano* **2016**, *10*, 3685–3692.
- (12) Qiu, H.; Zeng, X. C.; Guo, W. Water in inhomogeneous nanoconfinement: coexistence of multilayered liquid and transition to ice nanoribbons. *ACS Nano* **2015**, *9*, 9877–9884.
- (13) Agrawal, K. V.; Shimizu, S.; Drahushuk, L. W.; Kilcoyne, D.; Strano, M. S. Observation of Extreme Phase Transition Temperatures of Water Confined Inside Isolated Carbon Nanotubes. *Nat. Nanotechnol.* **2017**, *12*, 267–273.
- (14) Köfinger, J.; Hummer, G.; Dellago, C. Macroscopically Ordered Water in Nanopores. *Proc. Natl. Acad. Sci. U.S.A.* **2008**, *105*, 13218–13222.
- (15) Radha, B.; Esfandiar, A.; Wang, F.; Rooney, A.; Gopinadhan, K.; Keerthi, A.; Mishchenko, A.; Janardanan, A.; Blake, P.; Fumagalli, L.; et al. Molecular Transport Through Capillaries Made with Atomic-Scale Precision. *Nature* **2016**, *538*, 222–225.
- (16) Raju, M.; van Duin, A.; Ihme, M. Phase Transitions of Ordered Ice in Graphene Nanocapillaries and Carbon Nanotubes. *Sci. Rep.* **2018**, *8*, 3851.
- (17) Chen, J.; Schusteritsch, G.; Pickard, C. J.; Salzmann, C. G.; Michaelides, A. Two Dimensional Ice from First Principles: Structures and Phase Transitions. *Phys. Rev. Lett.* **2016**, *116*, 025501.
- (18) Ball, P. Water - an enduring mystery. *Nature* **2008**, *452*, 291–292.
- (19) Hua, L.; Huang, X.; Liu, P.; Zhou, R.; Berne, B. J. Nanoscale dewetting transition in protein complex folding. *J. Phys. Chem. B* **2007**, *111*, 9069–9077.
- (20) Klein, E.; Ferrand, Y.; Barwell, N. P.; Davis, A. P. Solvent effects in carbohydrate binding by synthetic receptors: implications for the role of water in natural carbohydrate recognition. *Angew. Chem.* **2008**, *47*, 2693–2696.
- (21) Won, C. Y.; Aluru, N. Structure and Dynamics of Water Confined in a Boron Nitride Nanotube. *J. Phys. Chem. C* **2008**, *112*, 1812–1818.
- (22) Shayeganfar, F.; Beheshtian, J.; Shahsavari, R. First-principles study of water nanotubes captured inside carbon/boron nitride nanotubes. *Langmuir* **2018**, *34*, 11176–11187.
- (23) Wagemann, E.; Wang, Y.; Das, S.; Mitra, S. K. On the Wetting Translucency of Hexagonal Boron Nitride. *Phys. Chem. Chem. Phys.* **2020**, *22*, 7710–7718.
- (24) Li, H.; Zeng, X. C. Wetting and Interfacial Properties of Water Nanodroplets in Contact with Graphene and Monolayer Boron-Nitride Sheets. *ACS Nano* **2012**, *6*, 2401–2409.
- (25) Kayal, A.; Chandra, A. Water in confinement between nanowalls: Results for hexagonal boron nitride versus graphene sheets from ab initio molecular dynamics. *J. Phys. Chem. C* **2019**, *123*, 6130–6140.
- (26) Giannozzi, P.; et al. QUANTUM ESPRESSO: A Modular and Open-Source Software Project for Quantum Simulations of Materials. *J. Phys.: Condens. Matter* **2009**, *21*, 395502.
- (27) Dion, M.; Rydberg, H.; Schröder, E.; Langreth, D. C.; Lundqvist, B. I. Van der Waals Density Functional for General Geometries. *Phys. Rev. Lett.* **2004**, *92*, 246401.
- (28) Langreth, D. C.; et al. A Density Functional for Sparse Matter. *J. Phys.: Condens. Matter* **2009**, *21*, 084203.

- (29) Rappe, A. M.; Rabe, K. M.; Kaxiras, E.; Joannopoulos, J. Optimized Pseudopotentials. *Phys. Rev. B: Condens. Matter Mater. Phys.* **1990**, *41*, 1227.
- (30) Monkhorst, H. J.; Pack, J. D. Special Points for Brillouin-Zone Integrations. *Phys. Rev. B: Solid State* **1976**, *13*, 5188.
- (31) Plimpton, S. Fast Parallel Algorithms for Short-Range Molecular Dynamics. *J. Comput. Phys.* **1995**, *117*, 1–19.
- (32) Berendsen, H.; Grigera, J.; Straatsma, T. The Missing Term in Effective Pair Potentials. *J. Phys. Chem.* **1987**, *91*, 6269–6271.
- (33) Wu, Y.; Wagner, L. K.; Aluru, N. R. Hexagonal Boron Nitride and Water Interaction Parameters. *J. Chem. Phys.* **2016**, *144*, 164118.
- (34) Hilder, T. A.; Yang, R.; Ganesh, V.; Gordon, D.; Bliznyuk, A.; Rendell, A. P.; Chung, S.-H. Validity of Current Force Fields for Simulations on Boron Nitride Nanotubes. *Micro Nano Lett.* **2010**, *5*, 150–156.
- (35) Mark, P.; Nilsson, L. Structure and Dynamics of the TIP3P, SPC, and SPC/E Water Models at 298 K. *J. Phys. Chem. A* **2001**, *105*, 9954–9960.
- (36) Martínez Gordillo, R.; et al. Atomistic Simulations in Hybrid C/BN Structures, PhD Thesis; Universitat Autònoma de Barcelona, 2014; p 92.
- (37) Leenaerts, O.; Partoens, B.; Peeters, F. Adsorption of H₂O, NH₃, CO, NO₂, and NO on Graphene: A First-Principles Study. *Phys. Rev. B: Condens. Matter Mater. Phys.* **2008**, *77*, 125416.
- (38) Li, S.; Schmidt, B. Two-Dimensional Water in Graphene Nanocapillaries Simulated with Different Force Fields: Rhombic Versus Square Structures, Proton Ordering, and Phase Transitions. **2019**, arXiv:1901.04236, e-Print Arch., Phys, 1–40.
- (39) Yamanaka, A.; Okada, S. Energetics and Electronic Structure of h-BN Nanoflakes. *Sci. Rep.* **2016**, *6*, 30653.
- (40) Booth, F. The Dielectric Constant of Water and the Saturation Effect. *J. Chem. Phys.* **1951**, *19*, 391.
- (41) Ritos, K.; Borg, M. K.; Mottram, N. J.; Reese, J. M. Electric Fields can Control the Transport of Water in Carbon Nanotubes. *Philos. Trans. R. Soc., A* **2016**, *374*, 20150025.
- (42) Winarto; Yamamoto, E.; Yasuoka, K. Water Molecules in a Carbon Nanotube under an Applied Electric Field at Various Temperatures and Pressures. *Water* **2017**, *9*, 473.
- (43) Winarto; Takaiwa, D.; Yamamoto, E.; Yasuoka, K. Structures of Water Molecules in Carbon Nanotubes under Electric Fields. *J. Chem. Phys.* **2015**, *142*, 124701.
- (44) Su, J.; Guo, H. Control of Unidirectional Transport of Single-File Water Molecules through Carbon Nanotubes in an Electric Field. *ACS Nano* **2011**, *5*, 351–359.
- (45) Bratko, D.; Daub, C. D.; Luzar, A. Water-mediated Ordering of Nanoparticles in an Electric Field. *Faraday Discuss.* **2009**, *141*, 55–66.
- (46) Wu, S.; et al. Magnetotransport Properties of Graphene Nanoribbons with Zigzag Edges. *Phys. Rev. Lett.* **2018**, *120*, 216601.

□ Recommended by ACS

Drastically Reduced Thermal Conductivity in Chlorinated Diamane due to the Emergence of Extremely Low-Frequency Optical Phonons

Tingting Zhang, Liyan Zhu, et al.

OCTOBER 21, 2022

THE JOURNAL OF PHYSICAL CHEMISTRY C

READ ▶

Coupled Evolution of Sliding and Rolling of Carbon Nanotubes: Effect of Lattice Mismatch and Size

Zhilin Luo and Wang Gao

JANUARY 12, 2023

THE JOURNAL OF PHYSICAL CHEMISTRY C

READ ▶

Amplifying Quantum Tunneling Current Sensitivity through Labeling Nucleotides Using Graphene Nanogap Electrodes

Sneha Mittal, Biswarup Pathak, et al.

JULY 13, 2022

ACS APPLIED NANO MATERIALS

READ ▶

Theoretical Rovibrational Characterization of Si₃O₃ and Mg₂O₃; Intermediates between Small Molecules and Nanocrystals

E. Michael Valencia and Ryan C. Fortenberry

SEPTEMBER 14, 2022

ACS EARTH AND SPACE CHEMISTRY

READ ▶

Get More Suggestions >